Original article

Nuclear Medicine Communications

Quantification and reduction of respiratory induced artifacts in positron emission tomography/computed tomography using the time-of-flight technique

Roya Sharifpour[a,b], Pardis Ghafarian[c,d], Arman Rahmim[e,f] and Mohammad R. Ay[a,b]

Objective **The aim of this study was to investigate the impact of time-of-flight (TOF) on quantification and reduction of respiratory artifacts.**

Patients and methods **The National Electrical Manufacturers Association phantom was used for optimization of reconstruction parameters. Twenty seven patients with lesions located in the diaphragmatic region were evaluated. The PET images were retrospectively reconstructed using non-TOF (routine protocol in our department) and TOF algorithms with different reconstruction parameters. Maximum standardized uptake value, estimated maximum tumor diameter, coefficient of variation, signal-to-noise ratio, and lesion-to-background-ratio were also evaluated.**

Results **On the basis of phantom experiments, TOF algorithms with two iterations, 18 subsets, and 5.4 mm and 6.4 mm postsmoothing filter reduced the noise by 3.1 and 12.6% in phantom with 2 : 1 activity ratio, and 3.0 and 13.1% in phantom with 4 : 1 activity ratio. The TOF algorithm with two iterations, 18 subsets, and 6.4 mm postsmoothing filter had the highest signal-to-noise value, and was selected as the optimal TOF reconstruction. Mean relative difference for signal-to-noise between non-TOF and optimal TOF in phantom with 2 : 1 and 4 : 1 activity ratio were 11.6 and 18.7%, respectively. In clinical data, the mean relative difference for estimated maximum tumor diameter and maximum standardized uptake value between routine protocol and optimal TOF algorithm were − 6.3% (range: − 20.4 to − 0.6%) and 13.2% (range: 0.3–57.6%), respectively.**

Conclusion **Integration of TOF in reconstruction algorithm remarkably improved the white band artifact in the diaphragmatic region. This technique affected the quantification accuracy and resulted in smaller tumor size and higher standardized uptake value in tumors located in/near the diaphragmatic region.** ***Nucl Med Commun*** **38:948–955**

Nuclear Medicine Communications 2017, **38**:948–955

Keywords: ^{18}F-FDG PET/CT, lesion size, quantification, respiratory artifact, standardized uptake value, time-of-flight

[a]Department of Medical Physics and Biomedical Engineering, [b]Research Center for Molecular and Cellular Imaging, Tehran University of Medical Sciences, [c]Chronic Respiratory Diseases Research Center, National Research Institute of Tuberculosis and Lung Diseases (NRITLD), Shahid Beheshti University of Medical Sciences, [d]PET/CT and Cyclotron Center, Masih Daneshvari Hospital, Shahid Beheshti University of Medical Sciences, Tehran, Iran, Departments of [e]Radiology and [f]Electrical and Computer Engineering, Johns Hopkins University, Baltimore, Maryland, USA

Correspondence to Pardis Ghafarian, PhD, Chronic Respiratory Diseases Research Center, National Research Institute of Tuberculosis and Lung Diseases (NRITLD), Shahid Beheshti University of Medical Sciences, Tehran 19569-44413, Iran
Tel/fax: + 98 912 504 7908/ + 98 212 610 9484;
e-mail: pardis.ghafarian@sbmu.ac.ir

Received 9 March 2017 **Revised** 5 August 2017 **Accepted** 7 August 2017

Introduction

Fluorine-18-fluorodeoxyglucose (^{18}F-FDG) PET/CT is an important noninvasive imaging tool for tumor detection, staging, and the therapy response evaluation in oncology patients [1,2]. Furthermore, quantitative PET/CT imaging enables prediction of response to therapy and prognostication of patient survival [3–8]. Nowadays, significant improvements of hardware and software in new-generation PET/CT scanners are introduced, including important reconstruction algorithm capabilities such as point spread function (PSF) modeling [9] and time-of-flight (TOF) [10,11].

PSF modeling can improve spatial resolution throughout the entire field of view (FOV). The improvement of image contrast [12], spatial resolution, and increased signal-to-noise ratios (SNR) are also observed in some studies [13,14]. It was also interesting that in nodal staging of non-small-cell lung cancer, PSF modeling is preferred to conventional ordered subset expectation maximization (OSEM), and obtained higher sensitivity [15]. This algorithm can also increase standardized uptake value (SUV) in the range of 5–80% and improve the accuracy of SUV calculations [16–18]. It can also improve lesion detectability [19]. TOF PET technique is used in fast scintillator detectors such as lutetiumoxyorthosilicate and lutetium–yttrium oxyorthosilicate for calculating the time difference between the arrivals of two coincident photons with high precision [20]. The PET images reconstructed with TOF have demonstrated higher SNR [20–22] especially in obese patients [22,23] and faster

0143-3636 DOI: 10.1097/MNM.0000000000000732

convergence with higher contrast recovery [21,24]. TOF PET caused modification of the accuracy and precision of small lesion uptake value [25], better detection of small structures, better uniformity, less noise, and higher lesion contrast [21,26]. Prieto *et al.* [27] described the combination of PSF and TOF to be an optimal method for quantification, as well as small lesion detection. Akamatsu *et al.* [28] demonstrated that the combination of PSF and TOF caused SUV increase in lymph node metastases and improved lesion detectability compared with conventional OSEM algorithms. Using appropriate reconstruction parameters plays an important role for convenient qualitative and quantitative analysis with PSF and/or TOF [21,29].

It should be noted that significant increase in staff and patient dose [30] is observed in some PET/CT centers because of repeating computed tomography (CT) scan when faced with some artifacts in CT or PET/CT images (e.g. respiratory artifacts, metal artifacts, contrast agent artifacts), leading to quantitative bias and degradation of image quality and interpretation [20,31–34]. Respiratory artifacts, as a common artifact, degrade the quality and quantitative accuracy of PET/CT images [35,36]. Previous studies have shown that tumor size and SUV were changed because of respiratory effects, especially when tumors were located in the lower lobe of lungs and/or in the liver dome [37]. Apostolova *et al.* [38] have demonstrated that motion blurring in most solitary pulmonary nodules of up to 30 mm can produce SUV underestimation (≥30%) in ^{18}F-FDG PET/CT imaging. They stated that motion blurring correction is vital for accurate SUV calculation in solitary pulmonary nodules. Respiratory artifacts are caused by inconsistencies between diaphragm positions in PET and CT images, leading to errors in attribution of the attenuation coefficient in the lower lobe of the lung. Respiratory gating as an effective solution has been implemented and studied extensively [39,40]. Furthermore, some investigations have shown that TOF can also reduce respiratory artifacts [24,41], attributed to reduced propagation of errors when using TOF. Utilizing the TOF information in reconstruction process limits the probability of annihilation to a part of line of response, instead of the whole line of response. As a result, the dependencies between voxels are reduced, which decreases the noise propagation and leads to reduction of sensitivity to errors such as errors that occur in attenuation correction [42]. In the case of attenuation correction errors, such as the error caused by respiration, TOF information generates spatial weighting that augments the attenuation spatial weighting and, when contradictory, competes with them and corrects the data that have spatial positions inconsistent with their TOF information [41].

In many PET/CT centers, respiratory gating is not routinely used, and to the best of our knowledge there is no systematic investigation in using various reconstruction methods to correct respiratory artifacts in the lower lobe of lungs and in the liver dome. The aim of the present study is to quantify the influence of using the TOF algorithm with optimal reconstruction parameters in decreasing the respiratory artifact in the diaphragmatic region.

Patients and methods

Phantom study

In order to optimize the reconstruction parameters in TOF reconstruction algorithm, we used the National Electrical Manufacturers Association International Electrotechnical Commission body phantom with six spheres with diameters of 10, 13, 17, 22, 28, and 37 mm. The spheres were filled with ^{18}F-FDG solution of a 4 : 1 and 2 : 1 activity ratio compared with the background activity (5.31 kBq/ml).

PET/CT scanner

All PET/CT images were acquired using Discovery 690 VCT (GE Healthcare, Milwaukee, Wisconsin, USA) with 64-slice CT. The CT component consisted of 58 368 solid-state detector elements that were arranged in 912 channels × 64 rows. The PET scanner consisted of 24 detector rings with a total of 13 824 lutetium–yttrium oxyorthosilicate crystals and dimensions of 4.2 × 6.3 × 25 mm. The PET component had 157 mm axial FOV with coincidence time window of 4.9 ns, and with time resolution of TOF almost 500 ps.

Patient population

Twenty seven oncology patients were retrospectively evaluated (16 men and 11 women). The patient set comprised four lung cancer, four non-Hodgkin lymphoma, three Hodgkin lymphoma, two colon cancer, four renal cell carcinoma, one pancreatic cancer, one gastric cancer, three breast cancer, four esophageal cancer, and one unknown primary; all lesions were located in the diaphragmatic region, including the lower lobe of the lungs, liver, spleen, and stomach. A total of 75 lesions including 29 primary tumors and 46 metastatic lesions were evaluated. The mean age of patients was 55.0 ± 15.2 years (range, 28–71 years). Patients with fasting blood sugar level higher than 200 mg/dl were excluded from our study. The fasting period for the entire patients was between 6 and 8 h. A weight-adapted intravenous injection of 331.4 ± 71.0 MBq of ^{18}F-FDG was administered according to European Association of Nuclear Medicine guidelines [43] and the PET/CT scan was acquired after 60.8 ± 1.5 min uptake time.

Data acquisition and reconstruction protocol

Two anterior–posterior and lateral CT topograms were used for both imaging and planning using automatic exposure control purpose. In the next step, the CT images were obtained from vertex to mid-thigh, with tube voltage of 100–120 kVp (depending on patient BMI), pitch of 0.98 : 1, 1-s gantry rotation time, and

2.5-mm slice thickness along with smart mA protocol depending on body habitus. Subsequently, the emission images were acquired in list mode with 3 min/bed position. For fusion of PET and CT images, 3.75 mm CT slice thicknesses were reconstructed. The PET images were reconstructed with TOF [modified OSEM (VUE Point HD) + PSF + TOF] and without TOF [modified OSEM (VUE Point HD, GE Healthcare, Milwaukee, Wisconsin, USA)] + PSF (routine protocol in our department that is recommended by the manufacturer). The image matrix of 256 × 256 with 2.73 mm pixel size and a slice thickness of 3.75 mm were used in each reconstruction. The reconstruction parameters in phantom studies were three iterations, 18 subsets, and a Gaussian postfilter with full width at half maximum (FWHM) of 6.4 mm for non-TOF algorithm, and two iterations and 18 and 24 subsets for TOF algorithm. A Gaussian postfilter with FWHM of 4.4, 5.4, and 6.4 mm was also used for all TOF algorithms [21]. In this study, the phantom was used in order to optimize the reconstruction parameters. The clinical data were reconstructed with optimized parameters (two iterations, 18 subsets, and 6.4 mm filter) to evaluate the implementation of TOF for reduction of respiratory induced artifact in the diaphragmatic region in the absence of respiratory gating device in PET/CT imaging.

Assessment strategy

For assessment of image quality and quantitative analysis for the various reconstruction methods in PET/CT images, the coefficient of variation (COV), SNR, and lesion-to-background ratio (L/B) in addition to semiquantitative analysis (SUV) were computed and studied. In order to calculate COV in the phantom study, 12 spherical volumes of interest (VOIs) with 30 mm diameter on the central slice and the slices ± 1, ± 2 away from the center (total of 60 VOIs) were depicted. However, in clinical data, the three spherical VOIs were put on the three axial slices around the largest and uniform liver section (total of nine VOIs), making sure not to include the portahepatis and major vessels [44]. The COV was measured as the ratio of the mean of the SD of VOIs and the mean of VOIs in the patient and phantom study, respectively. However, SNR was defined as the ratio of the maximum value of a VOI that encompasses the lesion minus the mean in background over the SD in the background. We also calculated L/B as the ratio of the maximum value of a VOI that encompasses the lesion over the mean in the background. For comparison among various reconstruction methods, we applied the relative difference of COV, SNR, and L/B between the specific reconstruction method and routine protocol. In clinical data, maximum SUV (SUV_{max}) (three-dimensional isocontour encompass the total lesion) is calculated by the definition of VOI for each lesion. Maximum tumor diameter as an indicator for lesion size was also estimated for all lesions. In order to estimate the maximum tumor diameter, first, the direction in which tumor had the largest size was chosen on the basis of the non-TOF image. Then the tumor profile was drawn and an appropriate Gaussian curve was fitted. The full width at half maximum of Gaussian curve is considered as the estimated maximum tumor diameter. The percentage of relative differences for SUV_{max} and estimated maximum tumor diameter was measured. The qualitative analysis was performed in addition to quantitative analysis by an expert physicians.

Statistical analysis

The normality of variables was evaluated by the Shapiro–Wilk method. Comparisons of different reconstruction algorithms were done by paired *t*-test if the normal distribution was observed and performed by Wilcoxon's signed-rank test for those without normal distribution. In all of the analyses, P less than 0.05 was considered to be statistically significant. Statistical analysis was performed using the SPSS package (SPSS, version 22.0; IBM Corp., Armonk, New York, USA).

Results

Figure 1 shows a transverse view of the National Electrical Manufacturers Association International Electrotechnical Commission body phantom with activity ratios of 2 : 1 (top) and 4 : 1 (bottom) reconstructed with various reconstruction methods. Obviously, the phantom with 4 : 1 activity ratio resulted in greater lesion conspicuity and reduced noise levels relative to the phantom with 2 : 1 activity ratio. The percentage of relative differences for COV, SNR, and L/B between non-TOF (routine protocol) and TOF algorithms are presented in Table 1. In both activity ratios, TOF2 (two iterations, 18 subsets, and 5.4 mm filter size) and TOF3 (two iterations, 18 subsets, and 6.4 mm filter size) led to lower noise levels. It was also observed that applying smaller filter sizes and higher subset number increased noise levels in the PET images. The higher improvement in SNR was observed for smaller subset and larger filter size (TOF3 with 18 subsets and 6.4 mm filter size). As Ferretti *et al.* [45] have shown in their study, we also observed that the implementation of TOF with higher subset and smaller filter size improved lesion to background ratio (TOF4 with 24 subsets and 4.4 mm filter size). In Fig. 2, the transverse and coronal views of a typical patient with respiratory artifacts reconstructed with non-TOF and optimized TOF technique are shown. It is clear that the respiratory artifact was reduced when TOF was utilized. It should be noted that using optimized TOF (two iterations, 18 subsets, and 6.4 mm filter size) decreased image noise and increased SNR value in comparison with routine protocol, so that the COV and SNR were 7.3% and 15.83 when using routine protocol and changed to 5.6% and 24.7 when TOF was used. The improvement in COV and SNR was statistically significant ($P < 0.01$). The impact of using TOF on the lesion size and SUV_{max} is evident in Figs 3 and 4, respectively. For all patients, the relative difference between non-TOF and optimized TOF for

Fig. 1

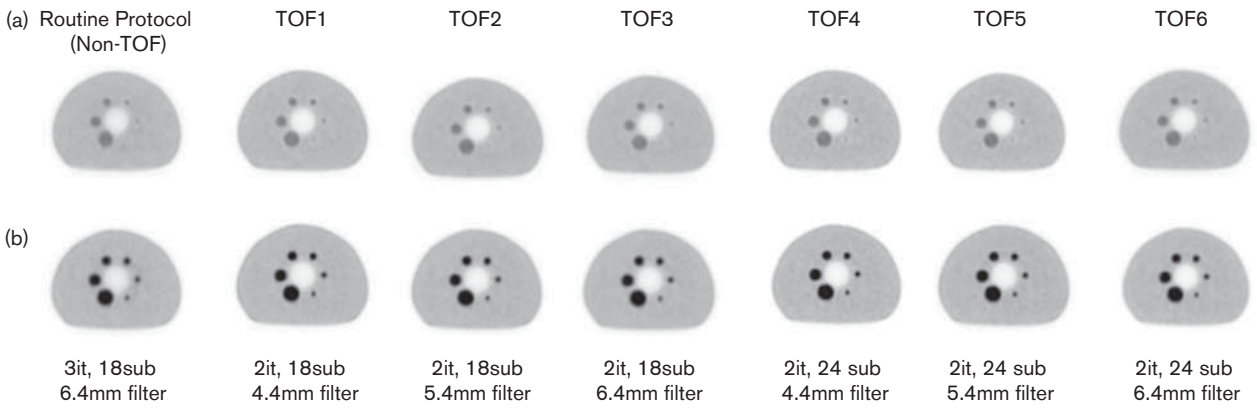

Various reconstructed PET images in transverse view of NEMA IEC body phantom with (a) 2 : 1 activity ratio and (b) 4 : 1 activity ratio. TOF, time-of-flight.

Table 1 The percentage of relative difference for image quality parameters between routine protocol (non-time-of-flight) and time-of-flight methods

	Phantoms					
	2 : 1			4 : 1		
Reconstruction methods	COV	SNR	L/B	COV	SNR	L/B
TOF1[a]	7.28	0.80	4.31	8.01	4.14	8.86
TOF2[b]	−3.08	7.11	1.67	−3.04	11.5	5.78
TOF3[c]	−12.6	11.6	−1.09	−13.1	18.7	2.26
TOF4[d]	27.5	−4.14	9.69	29.5	−8.97	12.9
TOF5[e]	13.5	0.52	6.17	14.8	−1.75	9.04
TOF6[f]	0.85	5.15	2.64	1.56	5.24	4.88

COV, coefficient of variation; L/B, lesion-to-background ratio; SNR, signal-to-noise ratios; TOF, time-of-flight.
[a]Two iterations, 18 subsets, 4.4 mm filter.
[b]Two iterations, 18 subsets, 5.4 mm filter.
[c]Two iterations, 18 subsets, 6.4 mm filter.
[d]Two iterations, 24 subsets, 4.4 mm filter.
[e]Two iterations, 24 subsets, 5.4 mm filter.
[f]Two iterations, 24 subsets, 6.4 mm filter.

Fig. 2

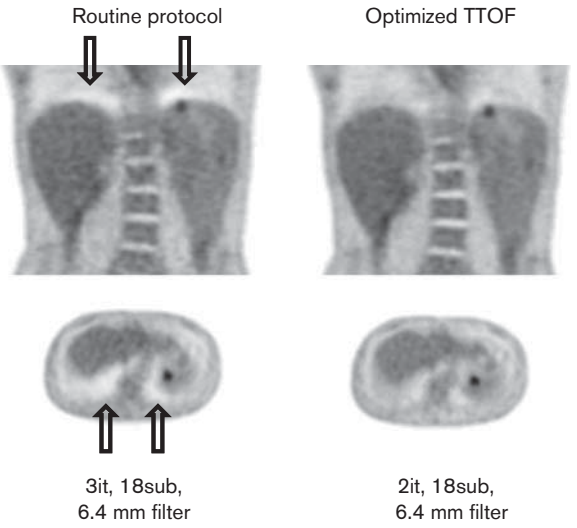

Reconstructed PET images in a 28-year-old man with esophageal cancer. Respiratory artifact reduction is obvious with the time-of-flight (TTOF) method. PET scan was done 59 min after administration of 286 MBq of fluorine-18-fluorodeoxyglucose.

estimated maximum tumor diameter illustrated the negative value in contrast to SUV_{max}. It means that implementing TOF led to lower lesion sizes and higher SUV_{max} values. In Fig. 5, the lung window of PET/CT images of a typical patient reconstructed with non-TOF and optimized TOF methods are shown. The higher image quality was observed for TOF in comparison with the non-TOF. Although 17.9 mm estimated maximum tumor diameter as seen in routine protocol, the estimated maximum tumor diameter in the optimized TOF method was 16.7 mm. The SUV_{max} increased from 3.68 in routine protocol to 4.74 in TOF.

Discussion

In order to reach the acceptable image quality in oncology patients in TOF PET/CT imaging, we used some optimal reconstruction parameters [21]. Our findings in this study showed that by increasing the filter size the noise level decreased, using various iteration and subsets, although higher noise level was observed by increasing the number of subsets, as Morey *et al.* [46] have suggested in their study. The noise level reached the least value when TOF algorithm with two iterations, 18 subsets, and 6.4 mm postfilter was applied. It should be clarified that in the patient data, by increasing the filter size, the SNR value increased with more impact when using smaller subsets (TOF3 with two iterations, 18 subsets, and 6.4 mm filter size). In addition, the combination of TOF and PSF produced a higher value of L/B compared with the routine protocol. SNR reduction

Fig. 3

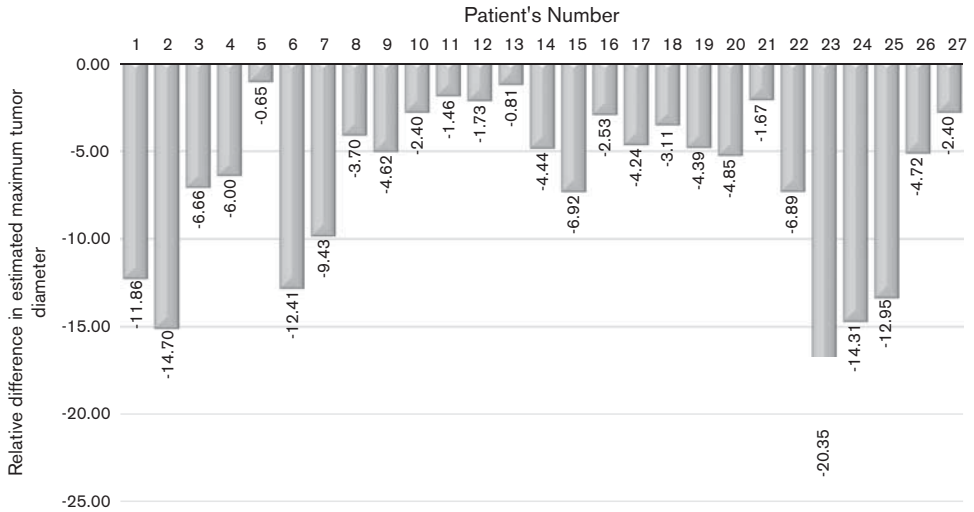

Mean relative difference in estimated maximum tumor diameter between routine protocol and optimized time-of-flight method in our clinical data.

Fig. 4

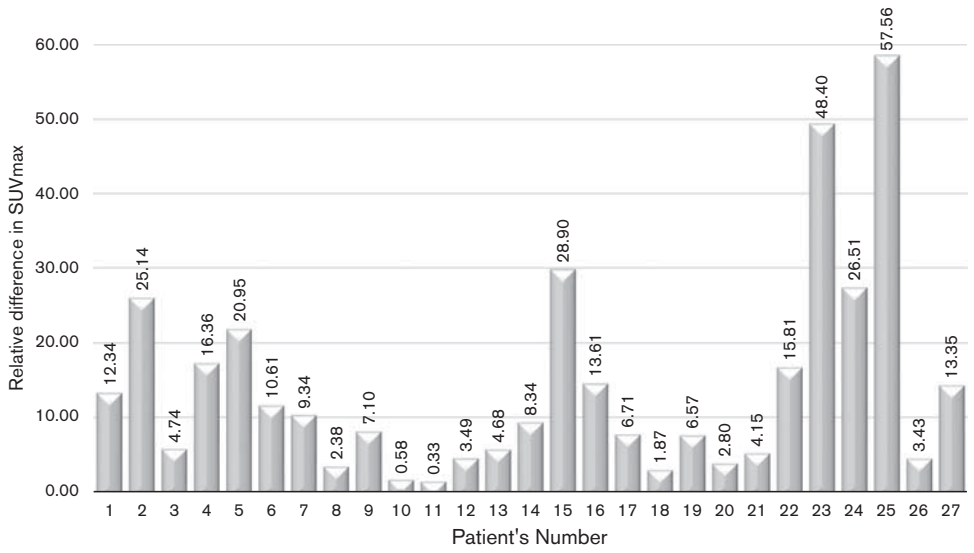

Mean relative difference in maximum standardized uptake value (SUV_{max}) between routine protocol and optimized time-of-flight method in our clinical data.

effects in thinner FWHM can lead to high contrast [47], as was seen in our findings. It would be noted that regarding all reconstruction methods used in the phantom study, considering SNR, COV, L/B, and overall image quality, the optimal image reconstruction method instead of the routine protocol [modified OSEM (VUE Point HD) + PSF] was modified OSEM (VUE Point HD) + PSF + TOF with two iterations, 18 subsets, and 6.4 mm in FWHM of the postsmoothing filter. It should be noted that using a gating device is an almost accurate method for reduction of respiratory artifact. Many studies have illustrated that because of lung motion in the PET imaging, the volume of lesions in the lungs and its vicinity is larger in nongated images compared with gated images [39,40]. Therefore, lesion size can be a proper indicator of respiratory artifact reduction. In our clinical study, TOF algorithm generated the smaller lesion sizes in comparison with the routine protocol that had a respiratory artifact as well. This finding proved that utilizing TOF in the reconstruction procedure can lead to

Fig. 5

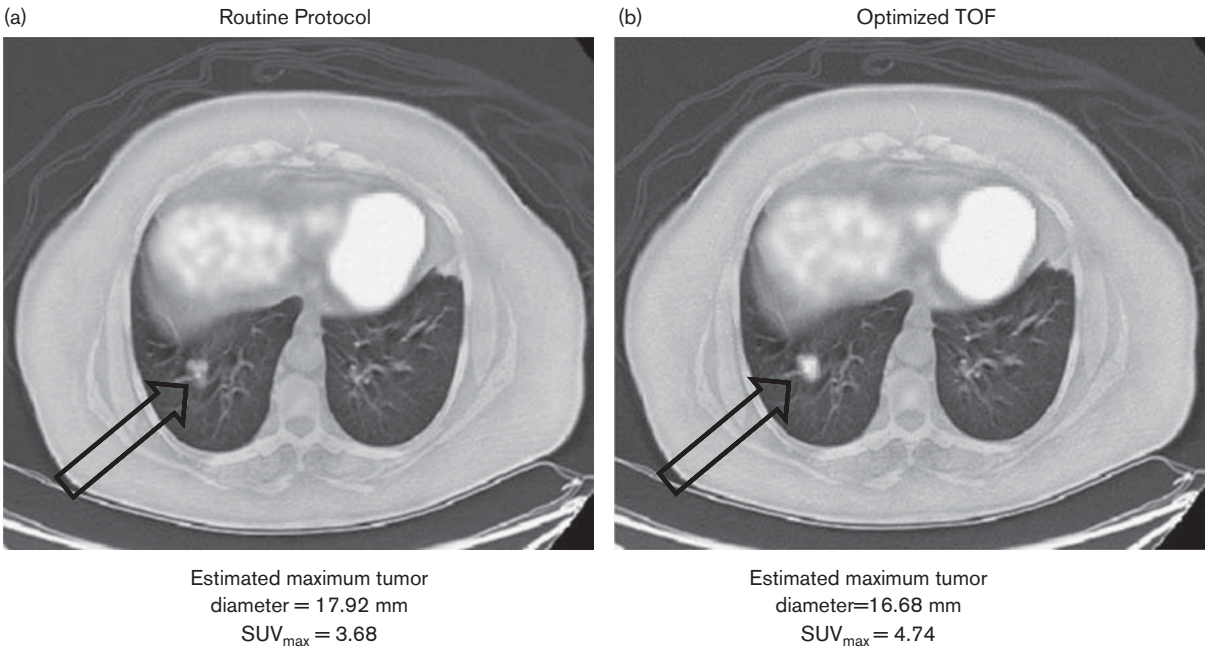

The impact of reconstruction methods on the maximum standardized uptake value (SUV_{max}) and estimated maximum tumor diameter in a 57-year-old woman with breast cancer. PET/CT images with regard to (a) routine protocol, (b) time-of-flight (TOF) with two iterations, 18 subsets, and 6.4 mm postfilter size. PET scan was done 61 min after administration of 375 MBq of fluorine-18-fluorodeoxyglucose.

respiratory artifact reduction. It would be interesting that the mean relative difference for lesion size between routine protocol and optimized TOF (two iterations, 18 subsets, and 6.4 mm postfilter size) was varied from −20.35 to −0.65%. On the basis of our clinical findings, TOF algorithm produced a higher SUV_{max} than the routine protocol. Mean relative differences for SUV_{max} between routine protocol and optimized TOF varied from 0.33 to 57.56%. It is noticeable that in qualitative analysis of clinical data the physicians confirmed that optimized TOF algorithm (two iterations, 18 subsets, and 6.4 mm postfilter size) depicted improved image quality in addition to lower respiratory artifact. We have to mention some limitations of our investigation. As the numbers of patients with lesions in the diaphragmatic region were low, we analyzed all of the lesions in this region without classification of the lesions into size groups and BMI especially for heavy and obese patients.

It is also worth noting that although PSF modeling is commonly reported to improve resolution, contrast, and lesion detection, as reported and referenced in the introduction, it also modifies the noise texture in the reconstructed images, and improvements in its performance actually depend on the task at hand and the imaging environment [48,49]. Upon reviewing the literature, we too have found that, in the presence of TOF, switching from no PSF to PSF modeling depicts greater improvement in performance than when TOF is absent [10,29,50]. As such, combined TOF + PSF can result in significantly improved clinical task performance.

Conclusion

In this study, the impact of TOF reconstruction on respiratory artifact was assessed and quantified. TOF resulted in a significant reduction of respiratory artifact and improved image quality. Quantitative parameters including SUV_{max} and tumor size were also significantly affected. Specifically, the reduction of blurring caused by respiration led to an average of −6.3% reduction in tumor size and increased SUV_{max} values by an average value of 13.2%. Our study suggests that using the TOF in reconstruction can improve the accuracy of quantitative analysis, through the reduction of respiratory artifact. In addition, because of the influence of TOF on quantitative parameters, the reconstruction method should be considered in reporting these parameters, especially in evaluation of response to therapy.

Acknowledgements

This work was supported under grant number 30848, Tehran University of Medical Sciences, as well as Masih Daneshvari Hospital and Shahid Beheshti University of Medical Sciences, Tehran, Iran.

Conflicts of interest

There are no conflicts of interest.

References

1 Wahl RL. *Principles and practice of PET and PET/CT*. Philadelphia, PA: Lippincott Williams & Wilkins; 2008.
2 Wahl RL, Jacene H, Kasamon Y, Lodge MA. From RECIST to PERCIST: evolving considerations for PET response criteria in solid tumors. *J Nucl Med* 2009; **50**:122s–150s.
3 Sheikhbahaei S, Wray R, Young B, Mena E, Taghipour M, Rahmim A, *et al*. ^{18}F-FDG-PET/CT therapy assessment of locally advanced pancreatic adenocarcinoma: impact on management and utilization of quantitative parameters for patient survival prediction. *Nucl Med Commun* 2016; **37**:231–238.
4 Marcus C, Antoniou A, Rahmim A, Ladenson P, Subramaniam RM. Fluorodeoxyglucose positron emission tomography/computerized tomography in differentiated thyroid cancer management: importance of clinical justification and value in predicting survival. *J Med Imag Radiat On* 2015; **59**:281–288.
5 Wray R, Marcus C, Sheikhbahaei S, Zan E, Ferraro R, Rahmim A, *et al*. Therapy response assessment and patient outcomes in head and neck squamous cell carcinoma: FDG PET Hopkins criteria versus residual neck node size and morphologic features. *Am J Roentgenol* 2016; **207**:641–647.
6 Maisonobe JA, Garcia CA, Necib H, Vanderlinden B, Hendlisz A, Flamen P, *et al*. Comparison of PET metabolic indices for the early assessment of tumour response in metastatic colorectal cancer patients treated by polychemotherapy. *Eur J Nucl Med Mol Imaging* 2013; **40**:166–174.
7 Tixier F, Hatt M, Valla C, Fleury V, Lamour C, Ezzouhri S, *et al*. Visual versus quantitative assessment of intratumor F-18-FDG PET uptake heterogeneity: prognostic value in non-small cell lung cancer. *J Nucl Med* 2014; **55**:1235–1241.
8 Lin C, Itti E, Haioun C, Petegnief Y, Luciani A, Dupuis J, *et al*. Early ^{18}F-FDG PET for prediction of prognosis in patients with diffuse large B-cell lymphoma: SUV-based assessment versus visual analysis. *J Nucl Med* 2007; **48**:1626–1632.
9 Rahmim A, Qi J, Sossi V. Resolution modeling in PET imaging: theory, practice, benefits, and pitfalls. *Med Phys* 2013; **40**:064301.
10 Kadrmas DJ, Casey ME, Conti M, Jakoby BW, Lois C, Townsend DW. Impact of time-of-flight on PET tumor detection. *J Nucl Med* 2009; **50**:1315–1323.
11 Karp JS, Surti S, Daube-Witherspoon ME, Muehllehner G. Benefit of time-of-flight in PET: experimental and clinical results. *J Nucl Med* 2008; **49**:462–470.
12 Bellevre D, Fournier CB, Switsers O, Dugué AE, Levy C, Allouache D, *et al*. Staging the axilla in breast cancer patients with ^{18}F-FDG PET: how small are the metastases that we can detect with new generation clinical PET systems? *Eur J Nucl Med Mol Imaging* 2014; **41**:1103–1112.
13 Tong S, Alessio A, Kinahan P. Noise and signal properties in PSF-based fully 3D PET image reconstruction: an experimental evaluation. *Phys Med Biol* 2010; **55**:1453.
14 Ahangari S, Ghafarian P, Shekari M, Ghadiri H, Bakhshayeshkaram M, Ay MR. The impact of point spread function modeling on scan duration in PET imaging. *Front Biomed Technol* 2015; **2**:137–145.
15 Lasnon C, Hicks RJ, Beauregard J-M, Milner A, Paciencia M, Guizard A-V, *et al*. Impact of point spread function reconstruction on thoracic lymph node staging with ^{18}F-FDG PET/CT in non-small cell lung cancer. *Clin Nucl Med* 2012; **37**:971–976.
16 Sheikhbahaei S, Marcus C, Wray R, Rahmim A, Lodge MA, Subramaniam RM. Impact of point spread function reconstruction on quantitative ^{18}F-FDG-PET/CT imaging parameters and inter-reader reproducibility in solid tumors. *Nucl Med Commun* 2016; **37**:288–296.
17 Hoetjes NJ, van Velden FH, Hoekstra OS, Hoekstra CJ, Krak NC, Lammertsma AA, *et al*. Partial volume correction strategies for quantitative FDG PET in oncology. *Eur J Nucl Med Mol Imaging* 2010; **37**:1679–1687.
18 Sharifpour R, Ghafarian P, Jamaati H, Doroudinia A, Ay MR. Impact of time-of-flight and point-spread-function for respiratory artifact reduction in PET/CT imaging: focus on SUV. *Tanaffos* (in press).
19 Kadrmas DJ, Casey ME, Black NF, Hamill JJ, Panin VY, Conti M. Experimental comparison of lesion detectability for four fully-3D PET reconstruction schemes. *IEEE Trans Med Imaging* 2009; **28**:523–534.
20 Geramifar P, Ay M, Zafarghandi MS, Sarkar S, Loudos G, Rahmim A. Investigation of time-of-flight benefits in an LYSO-based PET/CT scanner: a Monte Carlo study using GATE. *Nucl Instrum Methods Phys Res A* 2011; **641**:121–127.
21 Shekari M, Ghafarian P, Ahangari S, Ghadiri H, Bakhshayeshkaram M, Ay MR. Optimizing image reconstruction parameters in time of flight PET/CT imaging: a phantom study. *Front Biomed Technol* 2015; **2**:146–154.
22 El Fakhri G, Surti S, Trott CM, Scheuermann J, Karp JS. Improvement in lesion detection with whole-body oncologic time-of-flight PET. *J Nucl Med* 2011; **52**:347–353.
23 Surti S, Karp J. Experimental evaluation of a simple lesion detection task with time-of-flight PET. *Phys Med Biol* 2009; **54**:373–384.
24 Lois C, Jakoby BW, Long MJ, Hubner KF, Barker DW, Casey ME, *et al*. An assessment of the impact of incorporating time-of-flight information into clinical PET/CT imaging. *J Nucl Med* 2010; **51**:237–245.
25 Daube-Witherspoon ME, Surti S, Perkins AE, Karp JS. Determination of accuracy and precision of lesion uptake measurements in human subjects with time-of-flight PET. *J Nucl Med* 2014; **55**:602–607.
26 Shekari M, Ghafarian P, Ahangari S, Ay MR. Quantification of the impact of time of flight and point spread function on PET images using the noise matching concept: clinical and phantom study. *Nucl Sci Tech* (in press).
27 Prieto E, Domínguez-Prado I, García-Velloso MJ, Peñuelas I, Richter JÁ, Martí-Climent JM. Impact of time-of-flight and point-spread-function in SUV quantification for oncological PET. *Clin Nucl Med* 2013; **38**:103–109.
28 Akamatsu G, Mitsumoto K, Taniguchi T, Tsutsui Y, Baba S, Sasaki M. Influences of point-spread function and time-of-flight reconstructions on standardized uptake value of lymph node metastases in FDG-PET. *Eur J Radiol* 2014; **83**:226–230.
29 Akamatsu G, Ishikawa K, Mitsumoto K, Taniguchi T, Ohya N, Baba S, *et al*. Improvement in PET/CT image quality with a combination of point-spread function and time-of-flight in relation to reconstruction parameters. *J Nucl Med* 2012; **53**:1716–1722.
30 Zargan S, Ghafarian P, Monfared AS, Sharafi A, Bakhshayeshkaram M, Ay M. Evaluation of radiation exposure to staff and environment dose from [^{18}F]-FDG in PET/CT and cyclotron center using thermoluminescent dosimetry. *J BiomedPhys Eng* (in press).
31 Ahmadian A, Ay MR, Bidgoli JH, Sarkar S, Zaidi H. Correction of oral contrast artifacts in CT-based attenuation correction of PET images using an automated segmentation algorithm. *Eur J Nucl Med Mol Imaging* 2008; **35**:1812–1823.
32 Ghafarian P, Aghamiri S, Ay MR, Rahmim A, Schindler TH, Ratib O, *et al*. Is metal artefact reduction mandatory in cardiac PET/CT imaging in the presence of pacemaker and implantable cardioverter defibrillator leads? *Eur J Nucl Med Mol Imaging* 2011; **38**:252–262.
33 Abdoli M, Ay MR, Ahmadian A, Dierckx RA, Zaidi H. Reduction of dental filling metallic artifacts in CT-based attenuation correction of PET data using weighted virtual sinograms optimized by a genetic algorithm. *Med Phys* 2010; **37**:6166–6177.
34 Ay MR, Mehranian A, Abdoli M, Ghafarian P, Zaidi H. Qualitative and quantitative assessment of metal artifacts arising from implantable cardiac pacing devices in oncological PET/CT studies: a phantom study. *Mol Imaging Biol* 2011; **13**:1077–1087.
35 Ghafarian P, Ay MR, Fard-Esfahani A, Rahmim A, Zaidi H. Quantification of PET and CT misalignment errors due to bulk motion in cardiac PET/CT imaging: phantom and clinical and studies. *Front Biomed Technol* 2014; **1**:159–167.
36 Ghafarian P, Ay M. The influence of PET and CT misalignment due to respiratory motion on the cardiac PET/CT imaging: a simulation study. *Front Biomed Technol* 2015; **1**:252–257.
37 Geramifar P, Zafarghandi MS, Ghafarian P, Rahmim A, Ay MR. Respiratory-induced errors in tumor quantification and delineation in CT attenuation-corrected PET images: effects of tumor size, tumor location, and respiratory trace: a simulation study using the 4D XCAT phantom. *Mol Imaging Biol* 2013; **15**:655–665.
38 Apostolova I, Wiemker R, Paulus T, Kabus S, Dreilich T, van den Hoff J, *et al*. Combined correction of recovery effect and motion blur for SUV quantification of solitary pulmonary nodules in FDG PET/CT. *Eur Radiol* 2010; **20**:1868–1877.
39 Nehmeh SA, Erdi YE, Ling CC, Rosenzweig KE, Schoder H, Larson SM, *et al*. Effect of respiratory gating on quantifying PET images of lung cancer. *J Nucl Med* 2002; **43**:876–881.
40 Suzawa N, Ichikawa Y, Ishida M, Tomita Y, Nakayama R, Sakuma H. Respiratory-gated time-of-flight PET/CT during whole-body scan for lung lesions: feasibility in a routine clinical setting and quantitative analysis. *Ann Nucl Med* 2016; **30**:722–730.
41 Conti M. Why is TOF PET reconstruction a more robust method in the presence of inconsistent data? *Phys Med Biol* 2010; **56**:155.
42 Mehranian A, Zaidi H. Impact of time-of-flight PET on quantification errors in MR imaging–based attenuation correction. *J Nucl Med* 2015; **56**:635–641.
43 Boellaard R, Delgado-Bolton R, Oyen WJ, Giammarile F, Tatsch K, Eschner W, *et al*. FDG PET/CT: EANM procedure guidelines for tumour imaging: version 2.0. *Eur J Nucl Med Mol Imaging* 2015; **42**:328–354.
44 Fukukita H, Senda M, Terauchi T, Suzuki K, Daisaki H, Matsumoto K, *et al*. Japanese guideline for the oncology FDG-PET/CT data acquisition protocol: synopsis of Version 1.0. *Ann Nucl Med* 2010; **24**:325–334.

45 Ferretti A, Bellan E, Gava M, Chondrogiannis S, Massaro A, Nibale O, *et al*. Phantom study of the impact of reconstruction parameters on the detection of mini-and micro-volume lesions with a low-dose PET/CT acquisition protocol. *Eur J Radiol* 2012; **81**:3363–3370.
46 Morey AM, Kadrmas DJ. Effect of varying number of OSEM subsets on PET lesion detectability. *J Nucl Med Technol* 2013; **41**:268–273.
47 Sadick M, Molina F, Frey S, Piniol R, Sadick H, Brade J, *et al*. Effect of reconstruction parameters in high-definition PET/CT on assessment of lymph node metastases in head and neck squamous cell carcinoma. *J Nucl Med Technol* 2013; **41**:19–25.
48 Rahmim A, Tang J. Noise propagation in resolution modeled PET imaging and its impact on detectability. *Phys Med Biol* 2013; **58**:6945–6968.
49 Alessio A, Rahmim A, Orton CG. Resolution modeling enhances PET imaging (Point/Counterpoint). *Med Phys* 2013; **40**:120601.
50 Schaefferkoetter J, Casey M, Townsend D, El Fakhri G. Clinical impact of time-of-flight and point response modeling in PET reconstructions: a lesion detection study. *Phys Med Biol* 2013; **58**:1465–1478.